JOURNAL OF AIRCRAFT
Vol. 44, No. 5, September–October 2007

Experimental Aerodynamic Study of Tandem Flapping Membrane Wings

Jonathan Warkentin*
InvoDane Engineering, Ltd., Toronto, Ontario M3B 2T6, Canada
and
James DeLaurier†
University of Toronto, Toronto, Ontario M3H 5T6, Canada

DOI: 10.2514/1.28160

A systematic series of wind-tunnel tests was conducted on an ornithopter configuration consisting of two sets of symmetrically flapping wings, located one behind the other in tandem. It was discovered that the tandem arrangement can give thrust and efficiency increases over a single set of flapping wings for certain relative phase angles and longitudinal spacing between the wing sets. In particular, close spacing on the order of 1 chord length is generally best, and phase angles of approximately 0 ± 50 deg give the highest thrusts and propulsive efficiencies. Asymmetrical flapping was also studied, which consists of the two sets of wings rocking relative to one another 180 deg out of phase. It was found that the performance of such an arrangement is poor, relative to the best performing symmetrical tandem flapping.

I. Introduction

THE purpose of this work has been to evaluate the aerodynamic performance of tandem flapping wings, one directly behind the other. In particular, the lift, thrust, and propulsive efficiencies were measured for a range of reduced frequencies and phase angles between the two wings. The goal was to find conditions for optimum performance and to assess whether, under the right conditions, a benefit from mutual wake interference may occur.

Tandem-wing flapping is clearly inspired from the insect world. Dragonflies are one of nature's amazing solutions for hover, translational flight, and maneuverability. Such a solution is not found in the avian world (for reasons that are probably more compelling than aerodynamics alone), but the notion of tandem-wing ornithopters still persists for scales larger than insects. A major motivation is the idea of phasing the flapping to reduce the vertical oscillatory force imposed on the fuselage (Agrawal [1]), which is of particular importance for a piloted aircraft or one carrying motion-sensitive instrumentation (such as video equipment). A recent example of a tandem-wing ornithopter is the entomopter proposed by Michelson [2] for Mars exploration (Fig. 1). This aircraft uses a rocking-wing motion, which is a special case for tandem flapping (also studied in this work).

The key phenomenon that distinguishes tandem-wing flapping from the flapping of a single pair of wings is the wake interaction. Fairgrieve and DeLaurier [3] performed an analytical study of the wake generated by a single airfoil executing periodic but not necessarily harmonic motion. This did not include the shed leading-edge vortices that are characteristic of low Reynolds number flight (Ellington [4]), which were modeled for an oscillating airfoil by Zdunich [5] and Ansari, et al. [6]. An experimental wake study for single-wing flapping was conducted by Birch and Dickinson [7], which confirmed the leading-edge vortex hypothesis and provided information about its spanwise behavior. An important notion from this work is that the shed vortices may confer aerodynamic benefits on the wing itself at hover or near-hover conditions, especially at stroke reversal (Dickinson et al. [8]).

In light of this, it is a particularly intriguing hypothesis that, for tandem-wing flapping, the vortices shed from the forward wing may be used by the rearward wing to enhance the system's aerodynamic performance. Experimental studies on dragonflies by Somps and Luttges [9] clearly show the complex vortex interaction between the two wings, and one must assume that nature is benefiting from this fact. This notion is also shared by Azuma et al. [10] in their study of dragonfly flight mechanics.

This present research does not study, in great detail, the shed wakes or bound vortices. Instead, it concentrates on measuring the overall performance of tandem flapping wings under controlled wind-tunnel conditions and for specific ranges of variable parameters. These variables include distance between the wings, reduced frequencies (controlled by different flapping frequencies and wind speeds), and flapping phase angles. The measured values are average lift, thrust, and propulsive efficiency.

II. Experimental Apparatus

The experimental setup, shown in Figs. 2 and 3, is an electric-motor driven flapping mechanism supported in the test section of the University of Toronto Institute for Aerospace Studies wind tunnel. In particular, the mechanism consists of gear drives derived from a commercial model ornithopter, as shown in Fig. 4. A Mabuchi 370 electric motor operates, through a 56:1 gear train, cranks and rods attached to the large final-drive gears (on both sides). The rods are then attached, through ball joints, to the wing spars. In this way the high-speed rotary motion of the motor is converted to flapping oscillations at frequencies up to 7.5 Hz. The flapping rate is measured with an optical-break sensor in the main spur gear driving the forward wing (note that the aft wing is designed to flap at the same frequency as the forward wing).

The two sets of wings are coupled with toothed drive belts and timing pulleys (meshed to the final drive gears on both sides), and different belt lengths are used for different wing spacing. Further, the phase angles are readily changed by adjustment of the belts. Although most of the experiments consisted of symmetrical flapping (the left and right sets of wings flapped in a mirror-image fashion to the vertical longitudinal plane), the belt arrangement also allowed a close approximation to "rocking" flapping, where the wings act in a "teeter-totter" fashion, with the rear wing rocking 180 deg out of phase with the front wing.

Received 3 October 2006; revision received 29 March 2007; accepted for publication 30 March 2007.

*Flow Analyst, Research and Development, 30 Lesmill Road, Unit 2.
†Professor Emeritus, Institute for Aerospace Studies, 4925 Dufferin Street. Associate Fellow AIAA.

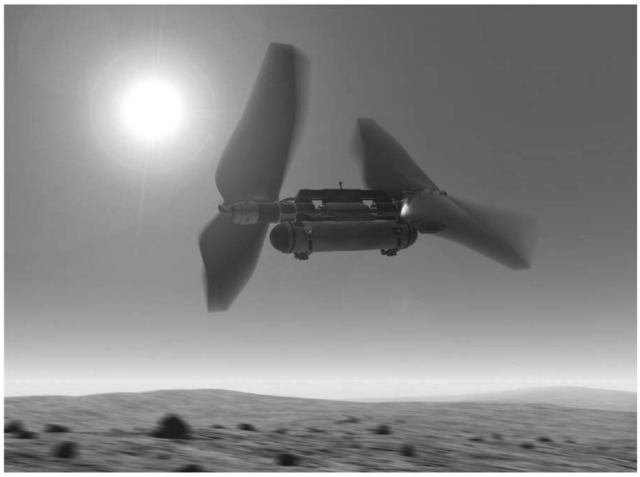

Fig. 1 Entomopter concept for Mars exploration.

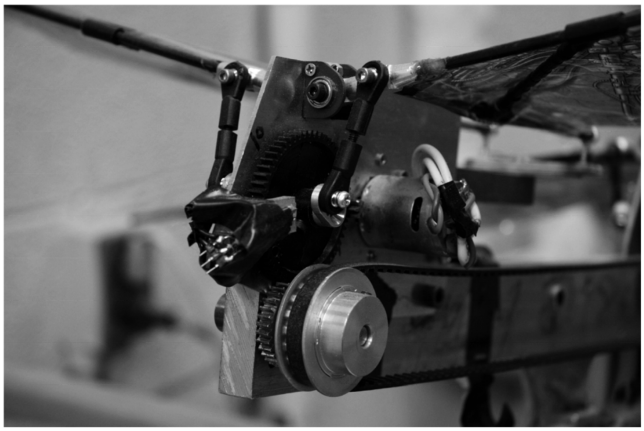

Fig. 4 Drive mechanism for wind-tunnel model.

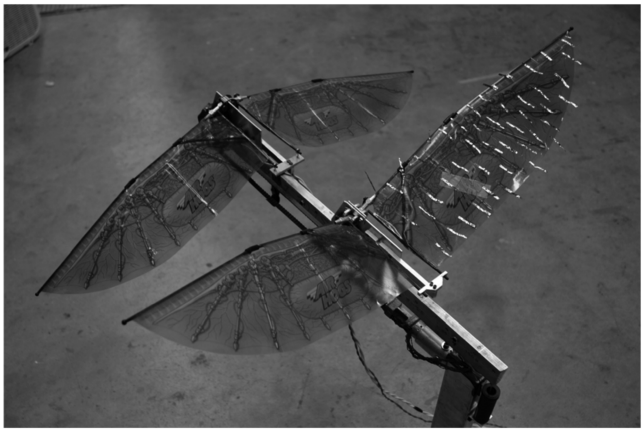

Fig. 2 Tandem-wing wind-tunnel model.

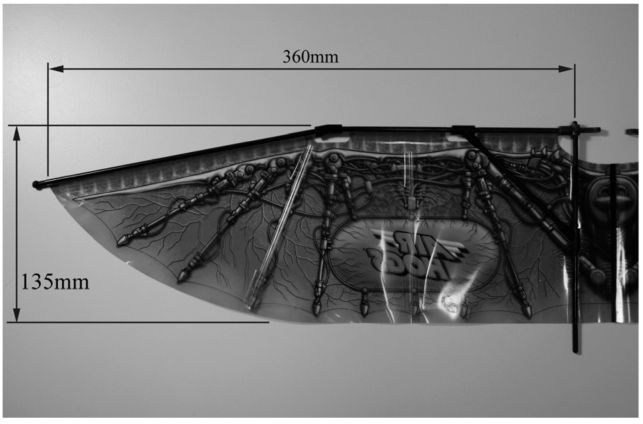

Fig. 5 Wing panel for wind-tunnel model.

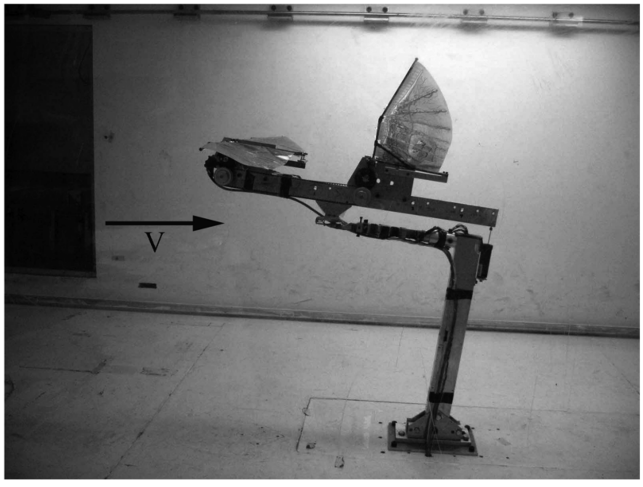

Fig. 3 Tandem-wing rig in wind tunnel.

The mechanism is mounted on a strain-gage balance, as seen in Fig. 3, from which the body-fixed axes readings of normal force, axial force, and pitching moment were obtained. These were converted, for the results, to the wind-axes values of lift and thrust. Pitching moment was not a consideration for this study. It should be noted that, based on the best calibration performed, the average error for thrust (also drag) is 6% and that for lift is 1%. The sources for error are dominated by the balance's zero drift, especially in the thrust direction.

The example wings were obtained from a commercial compressed-air powered model ornithopter (the "Cyberhawk," from the Spinmaster Corporation), and a wing panel is shown in Fig. 5. This was chosen because the model demonstrated excellent performance, and this seemed to be a worthy design for further study. These may be classified as "battened membrane wings," as opposed to the "shearflex" wings which incorporate a double-surface airfoil (described in [11]). The construction consists of a 3.5 mm diam carbon fiber/epoxy leading-edge spar from the flapping hinge to the midspan junction. From that point the spar is a 3.5 mm diam fiberglass rod. The membrane is 0.025 mm thickness Mylar, and the original battens were 4 mm diam hollow plastic straws (which were changed to stiffer pieces when the original battens folded during the higher frequencies). The printed design gives negligible weight, and the wing's total weight (left and right panels together) is 28.0 g.

To determine the propulsive efficiency, the power supplied to the flapping wings needs to be estimated. The source power supply provides the voltage and current to the electric drive motor. The power from this then goes through the gear-reduction drive and transfer belt to the connecting rods that flap the wings. The efficiency of this, minus the connecting rods, was measured with a dynamometer fabricated from a dc motor and a second power supply. The shaft of the dc motor was connected to the gear train's rear output shaft, and a calibrated strain-gauged lever arm was attached to the dc motor. Current is supplied to the dc motor, which gives a back torque to the rotating gear drive. This torque value, times the measured rotational rate, gives P_{flap} (the power available to flap the wings). The relation of output shaft power P_{flap} to the source power P_e is given by

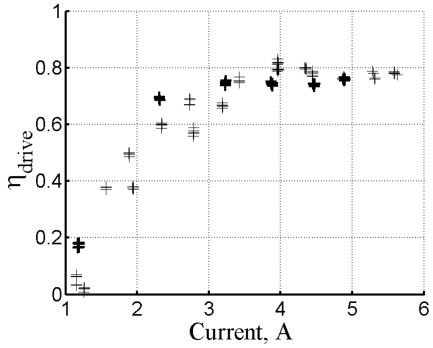

Fig. 6 Drive efficiencies for station 1.

$$P_{\text{flap}} = \eta_{\text{drive}} P_e$$

With this value, in relation to P_e, one may use the above equation to obtain the drive system's efficiency η_{drive}. A plot of the drive efficiency versus the source current, for the closest longitudinal position of the two sets of wings, is shown in Fig. 6.

It should be observed that these values ignore the power losses from the connecting rods and wing hinges, which would cause η_{drive} to be overestimated. Also, note that the dc motor simulates the backload from the wings, and this is measured at the rear output shaft where the rearward set of wings is driven. That is, the rearward set of wings is driven by a toothed belt from the front gear drive and motor, and the backloading torque was directly applied to the rear drive shaft. In an attempt to model the load carried by both drives, the rear drive was loaded to twice the estimated magnitude that would be encountered in the wind-tunnel tests. It was judged that the mechanical efficiency losses for such a setup would be somewhat larger than if the load had been divided between the two drive shafts. Therefore, this would cause η_{drive} to be underestimated, which may serve to compensate for the previous overestimation. In any case, these are considered to be a relatively small percentage of the total power losses, so that the measured values of η_{drive} are sufficiently accurate for the purposes of these experiments.

III. Parameters and Methodology

A key parameter for this study is the net average thrust T, measured in the wind-axis system (with tare drag subtracted). Upon extending the oscillating-wing thrust-coefficient definition from [12], this is nondimensionalized by

$$C_T = \frac{2T}{\rho V^2 S (2h_{\max}/c)^2}$$

where S is the total area of both sets of wings (0.1432 m^2), $2h_{\max}$ is the total arc distance traversed by the wing tips between full up and full down (0.34 m), and c is chosen to be the root chord (0.135 m). Observe that in these definitions there is no elastic bending, and both sets of wings go up 31 deg and down 23 deg (error of 1 deg) with an average dihedral angle of 4 deg.

The lift coefficient is defined in the usual way:

$$C_L = \frac{2L}{\rho V^2 S}$$

Also, the angle of attack α is defined to be the angle between the flapping axis and the freestream velocity. Note that when $\alpha = 0$, the weight of the wing's membrane surface creates an effective positive angle of attack that gives a small positive lift.

The propulsive efficiency is a measure of the wings' effectiveness in converting the supplied motor power to flight power, and the definition for these experiments is

$$\eta_p = \frac{P_{\text{out}}}{P_{\text{flap}}} = \frac{1}{\eta_{\text{drive}}} \frac{TV}{P_e}$$

where, as defined previously, η_{drive} is the combined efficiency of the motor, gear drive, and wing-actuation assembly when transferring power from electrical to mechanical means, and P_e is the source electrical power calculated as the motor's supply voltage multiplied by its supply current (thus η_{drive} is a function of current).

A differential method [13] is used to obtain the estimated error in η_p, the major sources of which are due to T and η_{drive}. Therefore, the error in the propulsive efficiency may be expressed as

$$e_{\eta_p} = \eta_p \left[\left(\frac{e_T}{T} \right)^2 + \left(\frac{e_{\eta_{\text{drive}}}}{\eta_{\text{drive}}} \right)^2 \right]^{1/2}$$

Another parameter is the reduced frequency k, which relates the velocity of the flow to the flapping rate

$$k = \frac{\pi f c}{V}$$

where f is in cycles per second. Another way to interpret k is through the "advance ratio" λ, which is the distance traveled in chord lengths per flapping cycle

$$\lambda = \frac{V}{fc} = \frac{\pi}{k}$$

The specific test variables are

1) Inverse of reduced frequency $1/k$, approximately over a range from 1 to 2.5.

2) Angles of attack α of 0, 6, and 12 deg.

3) Wind speed V of 3.3 m/s (except for one series at 5.0 m/s).

4) Longitudinal spacing between the wings of $0.39c$ (station 1), $1.126c$ (station 2), $1.90c$ (station 3), and $2.65c$ (station 4).

5) Phase angles ϕ, varying from 0 to 330 deg. Note that the zero value is when both wings are flapping in phase. Positive values are when the rear wing set is advanced relative to the front wing set. However, phase angles above 180 deg give the appearance of the rear set lagging the front set.

Each data point is the mean value for one test run. Because the zero drift is the main source of error, the error bars are chosen to be half of the zero drift from the beginning to the end of the run. Most runs were limited in duration to reduce the zero drift and therefore the error. Also, for each station, a repeatability test was performed to confirm the validity of the error estimate shown by the error bars.

IV. Results

A. Single Set of Flapping Wings

As a baseline case, a single pair of flapping wings was tested. The variables are as discussed previously, with a wind speed of 3.3 m/s. Also the reference area value, in this case only, is that for the single set of wings ($S = 716$ cm^2). Although the phase angle is irrelevant in this case, the rear drive was left on (at station 2) to give a correct value for η_{drive}.

The results for thrust coefficient, Fig. 7, show a uniform decrease with increasing $1/k$ (decreasing flapping frequency), as one would expect. Also, the thrust decreases as the angle of attack increases. This is similar behavior to the different membrane wings tested by Gallivan [14]. The lift-coefficient results (Fig. 8) remain fairly constant with $1/k$ though, as expected, these increase with angle of attack. Of particular interest are the propulsive-efficiency results shown in Fig. 9.

For the angles of attack tested, there are clear maximums at specific $1/k$ values. However,in no case are these above 12%. Even allowing for the fact that wing drag (induced and friction) is included in the efficiency calculation, this is not particularly efficient performance. This was surprising considering that the compressed-air flapping model, from which the wing was taken, flew very well with durations typically above 20 s.

Flow visualization was performed by attaching thin Mylar tufts to the upper surface of the wing. During the upstroke the tufts showed completely attached flow; but the downstroke demonstrated a

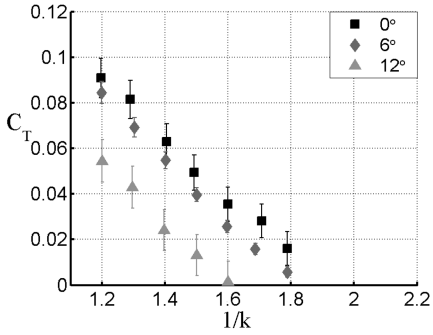

Fig. 7 Thrust coefficient vs $1/k$ for single-wing set.

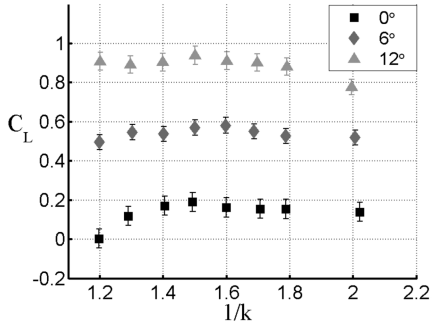

Fig. 8 Lift coefficient vs $1/k$ for single-wing set.

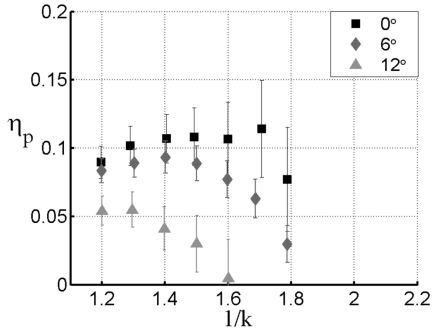

Fig. 9 Propulsive efficiency vs $1/k$ for single-wing set.

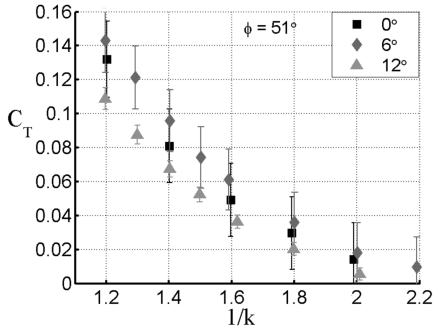

Fig. 10 Thrust coefficient vs $1/k$ for station 1.

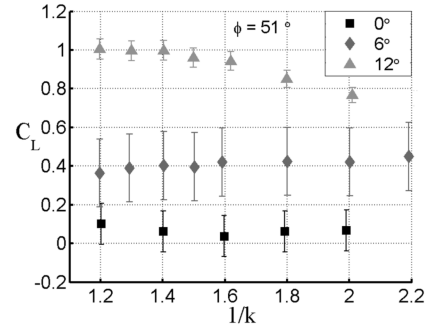

Fig. 11 Lift coefficient vs $1/k$ for station 1.

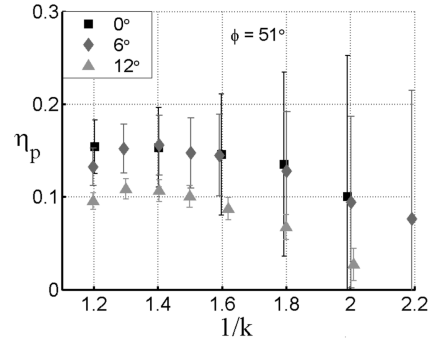

Fig. 12 Propulsive efficiency vs $1/k$ for station 1.

leading-edge bound vortex of the type described by Birch and Dickinson [7].

B. Stationary Rear Wing

The Schmidt wave propeller [15] uses a stationary rear wing to extract energy from a forward flapping wing. To study this effect with the present rig, the second set of wings was fixed (nonflapping) at station 2. It was found that the thrust performance was very poor, with the rear wings essentially just producing drag. This is not surprising because these wings have fairly sharp leading edges and thus produce negligible leading-edge suction. By comparison, the Schmidt design uses thick airfoils with significant leading-edge suction. Thus, the rear wing can use the crossflow component of the forward wing's wake to produce thrust.

C. Dual Set of Flapping Wings

Again, in this case, the wind speed was fixed at 3.3 m/s. A representative case, with $\phi = 51$ deg and station 1 positioning, is shown in Figs. 10–12. It is seen that the behavior is very similar to that for the single set of wings, though C_T is significantly larger (even allowing for the doubling of reference area, S).

Also, the lift coefficient varies a bit more with $1/k$ and the efficiency results clearly show a significant increase over the single-set case (with values up to 17%), which correlates with the improved thrust performance. However,the η_P error bars are large, which is a consequence of the measurement errors for C_T as well as those for η_{drive}. At the low currents required for low flapping frequencies (high values of $1/k$), η_{drive} has the largest errors.

The variation of the parameters with phase angle is of particular interest. For example, consider Figs. 13–16 which, for the four stations, show C_T vs ϕ at $1/k = 1.2$. Note that tests over the full range of α could only be conducted for the station 1 case. For the other station cases, the vibration of the rig was so excessive at $\alpha = 0$ deg that the measurement errors were unacceptable. Therefore, for comparison with the other stations, only results for $\alpha = 6$ and 12 deg are considered.

The station 1 results (Fig. 13) show that when the two sets of wings are closest, C_T varies over a factor of 2 (for $\alpha = 6$ deg) throughout the full range of ϕ values. The minimum thrust occurs when phase angle is approximately 230 deg, and the maximum is at phase angles close to zero (or 360 deg). Interestingly, Thomas et al. [16] in their

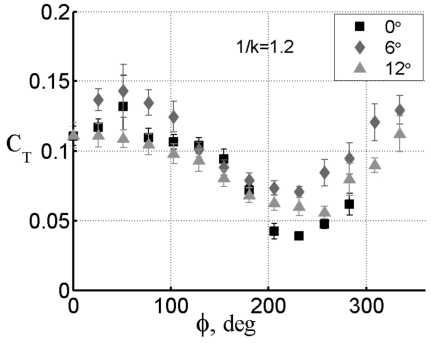

Fig. 13 Thrust coefficient vs phase angle for station 1.

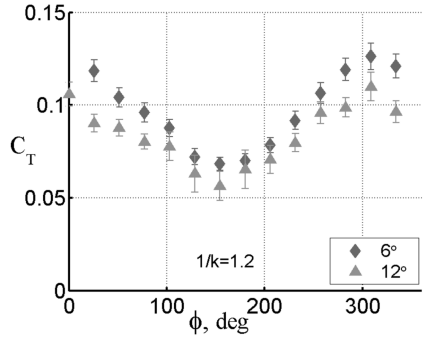

Fig. 14 Thrust coefficient vs phase angle for station 2.

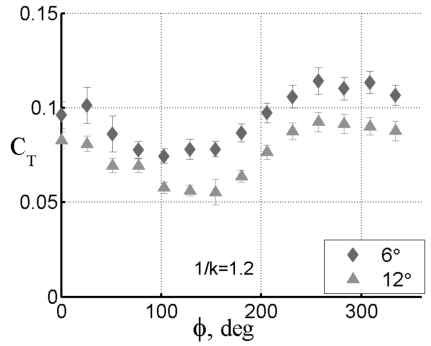

Fig. 15 Thrust coefficient vs phase angle for station 3.

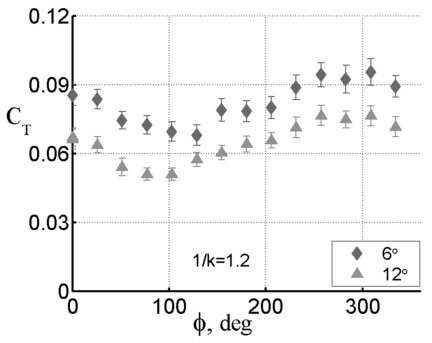

Fig. 16 Thrust coefficient vs phase angle for station 4.

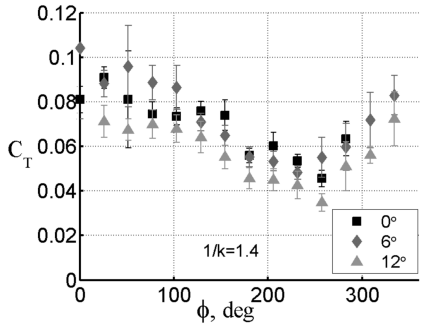

Fig. 17 Thrust coefficient vs phase angle for station 1.

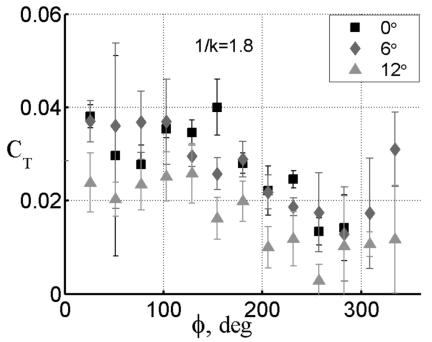

Fig. 18 Thrust coefficient vs phase angle for station 1.

studies of dragonfly flight, observed that nearly zero phase angles are used during high speed and maneuvering flight.

The station 2 case (Fig. 14), where the two sets of wings are further apart, show similar results. However,the maximum thrust coefficient is not quite as high. Further, these points shift to somewhat lower values of phase angles, with maximum thrust at $\phi \approx 310$ deg and minimum at $\phi \approx 150$ deg. This trend continues for station 3 (Fig. 15) and station 4 (Fig. 16). At the farthest distance (station 4), $(C_T)_{\max} \approx 0.095$ at $\alpha = 6$ deg, which is only 67% of the station 1 value of 0.141. Also, $(C_T)_{\max}$ occurs at $\phi \approx 280$ deg, and $(C_T)_{\min}$ occurs at $\phi \approx 130$ deg (for $\alpha = 6$ deg) and $\phi \approx 80$ deg (for $\alpha = 12$ deg).

Figure 17 shows C_T vs ϕ results, at station 1, for the lower flapping frequency of $1/k = 1.4$. The trends are similar to the $1/k = 1.2$ case, though the thrust magnitudes are less as expected. Also, although there is more scatter, it appears that the maximum and minimum values occur at approximately the same phase angles as before. At lower frequencies yet, the errors are too excessive (relative to the thrust magnitudes) to make clear statements about $(C_T)_{\max}$ and $(C_T)_{\min}$ locations. An example is Fig. 18 for $1/k = 1.8$. There is still evidence, though, of a trend similar to that for the higher-frequency results.

The variation of lift coefficient with phase angle is shown, for $1/k = 1.2$, in Figs. 19–22. As before, the data for $\alpha = 0$ deg is absent, except in the station 1 case where the magnitudes are small (as expected) and a clear maximum exists at $\phi \approx 150$ deg. At higher angles the C_L values become more constant, which is also the case for the station 2 results. Recall that these are averaged lift-coefficient values, and do not represent the variation of lift throughout the flapping cycle.

For the station 3 case (Fig. 21), the C_L values are less constant and show a mild "double-peak" behavior for the $\alpha = 6$ deg results. This digression is even more pronounced for the station 4 data (Fig. 22) which show a clear maximum at $\phi \approx 0$ deg (360 deg) and minimum at $\phi \approx 180$ deg. It is interesting that this mutual interference between the wings evidently becomes more pronounced as the distance increases. However,this may be due to the scale of the wake in relation to this distance.

The lift results for the four station cases at a lower flapping frequency ($1/k = 1.4$) closely match those previously described. The greatest difference is in the station 4 case (Fig. 23), where, in comparison with the $1/k = 1.2$ results, the variation with phase angle is not as great. In fact, for the lowest flapping frequency

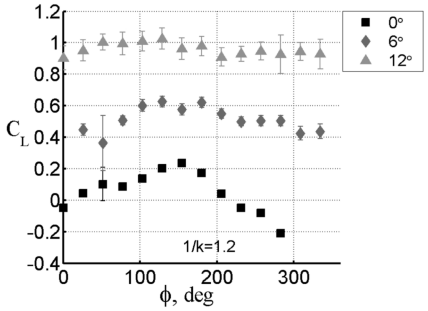

Fig. 19 Lift coefficient vs phase angle for station 1.

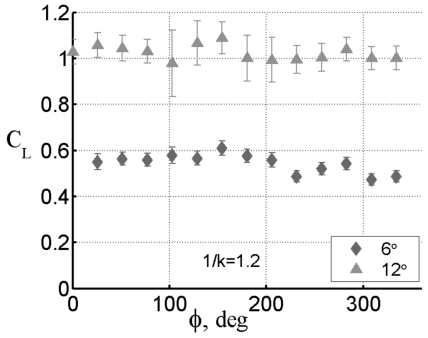

Fig. 20 Lift coefficient vs phase angle for station 2.

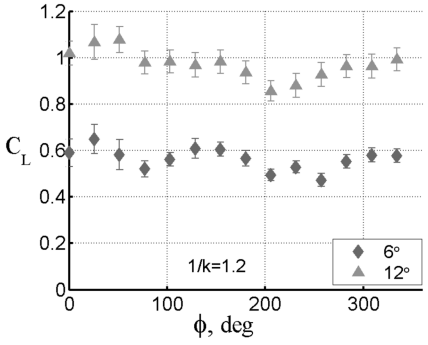

Fig. 21 Lift coefficient vs phase angle for station 3.

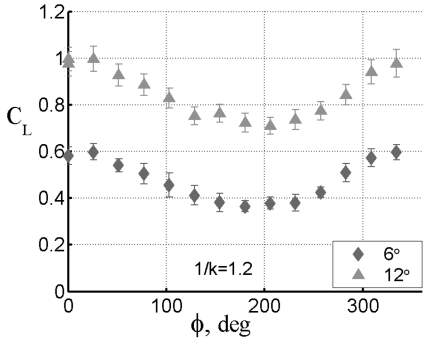

Fig. 22 Lift coefficient vs phase angle for station 4.

(1/k = 1.8), Fig. 24 shows very constant behavior. It may well be that the lower-energy vortices generated by this less-energetic flapping have less effect on the overall lift variation with phase angle.

The propulsive-efficiency results for 1/k = 1.2 are shown in Figs. 25–28. Just as with the thrust coefficients, these show a strong

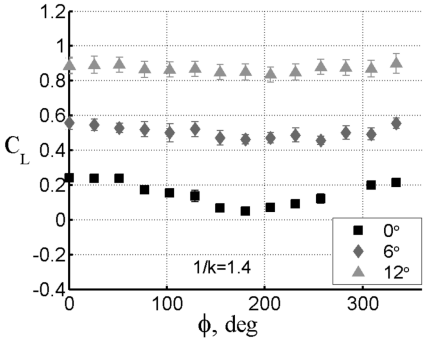

Fig. 23 Lift coefficient vs phase angle for station 4.

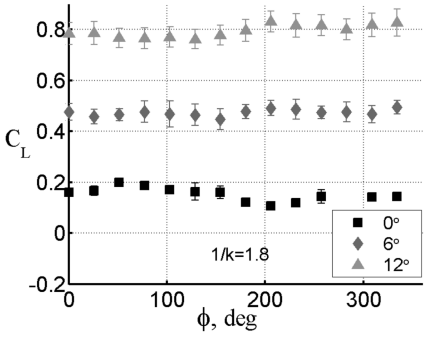

Fig. 24 Lift coefficient vs phase angle for station 4.

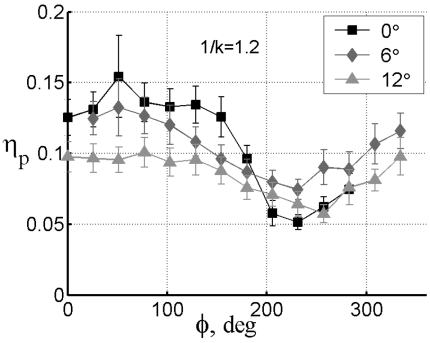

Fig. 25 Propulsive efficiency vs phase angle for station 1.

variation with phase angle. This is not surprising considering the dependence of η_P on C_T. The errors for calculating η_P are rather high, and are increasingly so for the lower frequencies (higher 1/k values). Therefore, only the 1/k = 1.2 results will be discussed. First of all, for station 1 (Fig. 25), the maximum efficiency values appear to be at $\phi \approx 50$ deg for all angles of attack. Also, upon comparing the maximum efficiencies to those for the single set of wings (Fig. 9), one sees a great improvement. For example, at $\alpha = 6$ deg the tandem-wing maximum efficiency equals 0.13, compared with the 0.09 value of the single set of wings.

The efficiency results are even better for the station 2 case (Fig. 26), where the peak values now occur at $\phi \approx 310$ deg. Also, for $\alpha = 6$ deg one has that $(\eta_P)_{\max} = 0.17$. This trend appears to continue to the station 3 case (Fig. 27), although the error bars are becoming too large to comfortably identify specific values. This is not so, however, for station 4 (Fig. 28), where the error bars are relatively small and one can see that $\phi \approx 310$ deg is also a point at which $(\eta_P)_{\max}$ occurs. However,because of the large distance between the wings, the maximum efficiencies are only somewhat larger than those for the single set of wings.

It is important to note that the exactly-out-of-phase condition of $\phi = 180$ deg is not a condition for either maximum thrust or

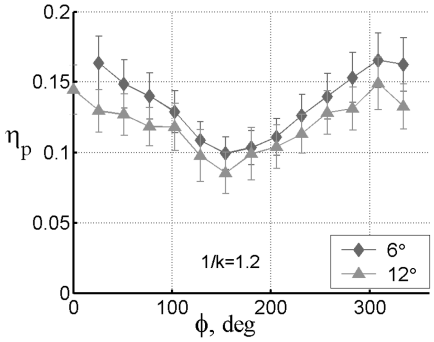

Fig. 26 Propulsive efficiency vs phase angle for station 2.

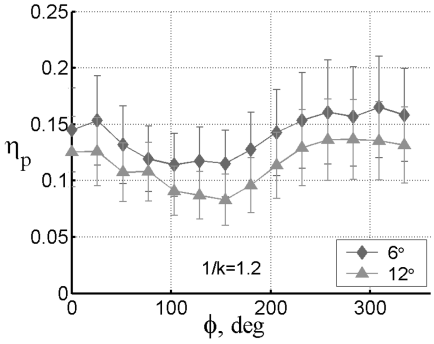

Fig. 27 Propulsive efficiency vs phase angle for station 3.

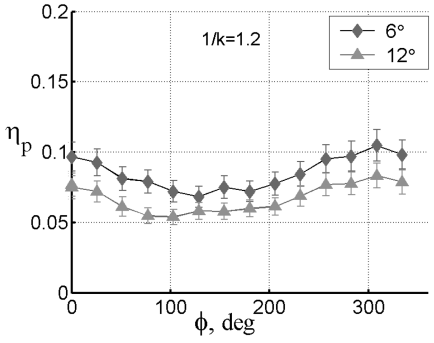

Fig. 28 Propulsive efficiency vs phase angle for station 4.

maximum efficiency. Also in some instances, as seen in Fig. 22, the average lift is significantly reduced. Therefore, unless the vertical-acceleration reduction promised by the $\phi = 180$ deg flapping condition is the most important design criteria, it appears that the flight performance of such an ornithopter would be seriously compromised.

D. Tandem Rocking Wings

Another flapping geometry that is appealing for vertical-acceleration reduction, as well as offering a certain mechanical simplicity, is the "rocking-wing" motion. In this case the wing structure across the flapping hinge is rigid, so that as one wing half rises the other half descends. This type of motion is seen in Fig. 1, and it was possible to replicate this with the existing rig by setting the phase angles of the wing halves 180 deg apart. Also, the front set of wings was phased 180 deg relative to the rear set.

The results from the experiments were compared with those for the symmetric-flapping cases with $\phi = 180$ deg, shown in Figs. 29–31. It is seen that, in general, the symmetric-flapping results outperform those for rocking-wing flapping. Although these may still lie within the two sets of error bars, the fact that rocking-wing performance is comparable to that for the nonoptimum symmetric-flapping case does not make this an attractive design feature.

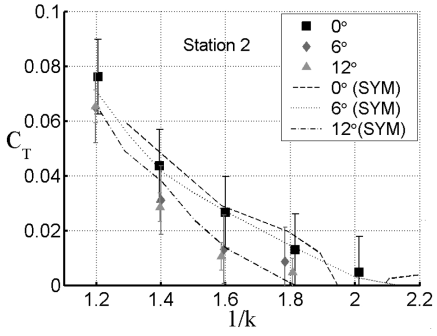

Fig. 29 Thrust coefficient vs $1/k$ for rocking wings.

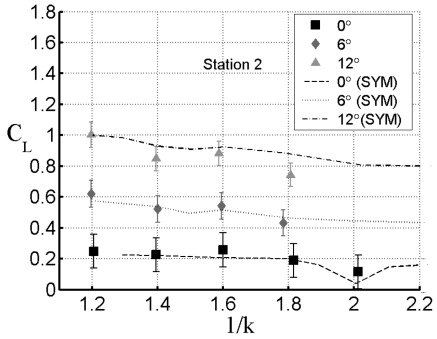

Fig. 30 Lift coefficient vs $1/k$ for rocking wings.

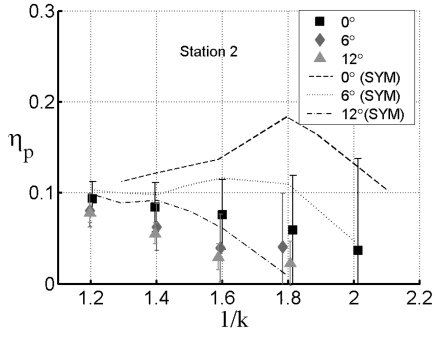

Fig. 31 Propulsive efficiency vs $1/k$ for rocking wings.

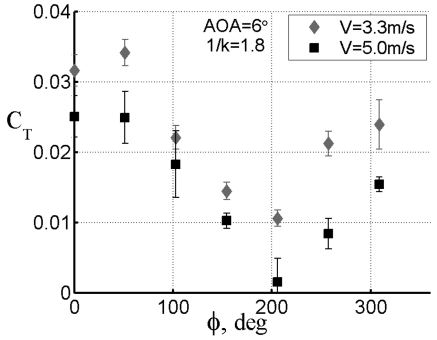

Fig. 32 Thrust coefficient vs phase angle for station 2.

E. Effect of Increased Wind Speed

Although almost all of the experiments were conducted at a wind-tunnel speed of 3.3 m/s, it was considered important to assess how higher dynamic pressures would affect the results. Therefore,

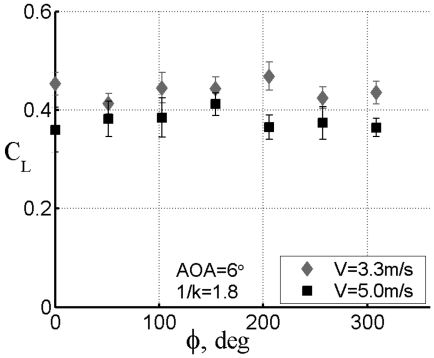

Fig. 33 Lift coefficient vs phase angle for station 2.

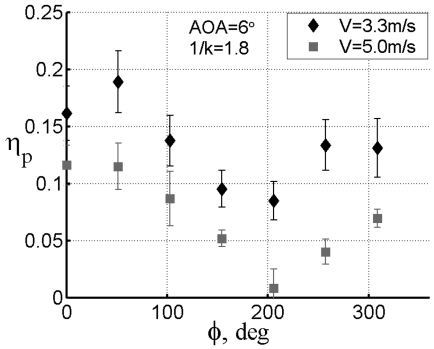

Fig. 34 Propulsive efficiency vs phase angle for station 2.

selected tests were conducted at $V = 5.0$ m/s. Only station 2 was chosen, with $\alpha = 6$ deg and $1/k = 1.8$. Consider the results shown in Figs. 32–34. The thrust coefficients are considerably lower for the higher speeds, even at the same reduced frequencies. This is largely due to the fact that the wings are flexible and that their bending and twisting geometries are much different under higher dynamic pressures. The average lift is less affected, though the propulsive efficiencies are greatly reduced in the same manner as the thrust coefficients. What should be noted, though, is that the variations with phase angle are much the same for the higher speeds as for the lower speeds. That is, the values of ϕ for optimum performance match those for the lower-speed cases.

V. Conclusions

This research has presented a systematic study of the average thrusts, lifts, and propulsive efficiencies of single-set and tandem flapping membrane wings of a given design. The variables have been flapping frequency and angle of attack, as well as longitudinal spacing and flapping phase angle between the wing sets. It was found that the optimum tandem-wing arrangement outperformed the single set of wings with efficiencies nearly twice as large. However,this came at phase angles ($\approx 0 \pm 50$ deg) that are not close to providing cancellation of vertical acceleration.

When compared with the results from studies of dragonflies, Thomas et al. [16] and Wakeling and Ellington [17] have observed maximum thrust at $\phi \approx 0$ deg and maximum efficiencies at $\phi \approx 90$ deg. These are comparable to the results from this study, considering that the wing layout for a dragonfly differs significantly (with variable longitudinal spacing along the span) from that for the model used in these experiments. Also, tandem-fin analysis of a swimming fish by Akhtar et al. [18] has shown a phase-angle range for optimum performance that closely matches the results from these experiments.

The magnitudes of the lift coefficients were similar between the single set and tandem sets of flapping wings (accounting for the differences in defined reference areas). The variation with frequency was not as great as that for the thrust coefficients. Generally, there was an increase with flapping frequency.

It was found that both station 1 (0.39c spacing) and station 2 (1.126c spacing) could give comparable performances in thrust, lift, and efficiency. However,beyond that, the thrust and lift performances would generally decrease so that at station 4 (2.65c spacing) the peak thrusts and efficiencies were nearly half those of the closer arrangements.

As for the rocking-wing configuration, although this would appear to offer advantages in mechanical implementation, its performance was comparable to the lowest values for symmetric flapping. Therefore, pending further studies, it does not appear to be attractive for optimum ornithopter design.

Finally it should be noted that only one wing-panel design was used for this study: a battened–stiffened membrane wing from a commercial flying model. Although the model flew well, this is by no means an endorsement of its being an optimum design. Therefore, the results could vary significantly for other wing designs. Further, the tandem-wing layout does not match the geometry of a dragonfly, which has very close longitudinal spacing (almost overlapping) at the root and wider spacing at the tip. The intention was to explore a tandem-wing arrangement that might be incorporated into an ornithopter. A direction for future research would be to explore variable spanwise spacing as well as different wing designs. A more fully battened semirigid wing panel may offer advantages at this scale. Another consideration for future experiments is to obtain a more accurate measure of the drive efficiency. This should include loading both the front and aft mechanisms in a realistic manner.

Aside from these caveats, it would appear that the present tests have pointed the way to some general rules for tandem-wing ornithopter design, as well as showing advantages these may have relative to a more traditional single set of flapping wings. What is particularly encouraging is how well these track with observations from nature.

Acknowledgment

The authors wish to acknowledge the support of the Natural Sciences and Engineering Research Council, through the Discovery Grant program.

References

[1] Agrawal, U., "Feasibility Studies of Non-Oscillatory Lift Generation Using a Tandem Flapping Wing Configuration," M.Sc. Thesis, University of Toronto Institute for Aerospace Studies, Jan. 2006.

[2] Michelson, R., "Novel Approaches to Miniature Flight Platforms," *Journal of Aerospace Engineering*, Special Issue, Vol. 218, 2004, pp. 363–373.

[3] Fairgrieve, J. D. and DeLaurier, J. D., "Propulsive Performance of Two-Dimensional Thin Airfoils Undergoing Large-Amplitude Pitch and Plunge Oscillations," Univ. of Toronto Inst. for Aerospace Studies Tech. Note No. 226, July 1982.

[4] Ellington, C. P., van den Berg, C., Willmott, A. P., and Thomas, A. L. R., "Leading-Edge Vortices in Insect Flight," *Nature (London)*, Vol. 384, Dec. 1996, pp. 626–630.

[5] Zdunich, P., "A Discrete Vortex Model of Unsteady Separated Flow About A Thin Airfoil for Application to Hovering Flapping-Wing Flight," M.Sc. Thesis, University of Toronto Institute for Aerospace Studies, 2002.

[6] Ansari, S. A., Zbikowski, R., and Knowles, K., "A Nonlinear Unsteady Aerodynamic Model for Insect-Like Flapping Wings in the Hover, Part 1," *Journal of Aerospace Engineering*, Vol. 220, No. 2, 2006, pp. 61–83.

[7] Birch, J. M., and Dickinson, M. H., "The Influence of Wing-Wake Interactions on the Production of Aerodynamic Forces in Flapping Flight," *Journal of Experimental Biology*, Vol. 206, March 2003, pp. 2257–2272.

[8] Dickinson, M. H., Lehmann, F.-O., and Sane, S. P., "Wing Rotation and the Aerodynamic Basis of Insect Flight," *Science*, Vol. 284, June 1999, pp. 1954–1960.

[9] Somps, C., and Luttges, M., "Dragonfly Flight: Novel Uses of Unsteady Separated Flows," *Science*, Vol. 228, June 1985, pp. 1326–1328.

[10] Azuma, A., Azuma, S., Watanabe, I., and Furuta, T., "Flight Mechanics of a Dragonfly," *Journal of Experimental Biology*, Vol. 116, Sept. 1985, pp. 79–107.

[11] DeLaurier, J. D., "The Development of an Efficient Ornithopter Wing," *Aeronautical Journal*, Vol. 97, May 1993, pp. 153–162.

[12] DeLaurier, J. D., and Harris, J. M., "Experimental Study of Oscillating-Wing Propulsion," *Journal of Aircraft*, Vol. 19, No. 5, May 1982, pp. 368–373.

[13] Salas, S., Hille, E., and Etgen, G., *Calculus: One and Several Variables*, 8th ed., Wiley, New York, 1999, pp. 934–939.

[14] Gallivan, P. A., "Wind Tunnel Testing of Various Designs for Flexible, Flapping, Membrane Wings," M.Sc. Thesis, Inst. for Aerospace Studies, Univ. of Toronto, 2005.

[15] Jones, K. D., and Platzer, M. F., "An Experimental and Numerical Investigation of Flapping-Wing Propulsion," AIAA Paper 99-0995, 1999.

[16] Thomas, A. L. R., Taylor, G. K., Srygley, R. B., Nudds, R. L., and Bomphrey, R. J., "Dragonfly Flight: Free-Flight and Tethered Flow Visualizations Reveal a Diverse Array of Unsteady Lift-Generating Mechanisms, Controlled Primarily via Angle of Attack," *Journal of Experimental Biology*, Vol. 207, No. 24, 2004, pp. 4299–4323.

[17] Wakeling, J. M., and Ellington, C. P., "Dragonfly Flight 2: Velocities, Accelerations and Kinematics of Flapping Flight," *Journal of Experimental Biology*, Vol. 200, Oct. 1996, pp. 557–582.

[18] Akhtar, I., Mittal, R., Lauder, G., and Drucker, E., "Hydrodynamics of a Biologically Inspired Tandem Flapping Foil Configuration," *Theoretical and Computational Fluid Dynamics* (to be published).